Regulation of Rho-Dependent Transcription Termination by NusG Is Specific to the *Escherichia coli* Elongation Complex†

Zvi Pasman and Peter H. von Hippel*

Institute of Molecular Biology and Department of Chemistry, University of Oregon, Eugene, Oregon 97403

Received November 17, 1999; Revised Manuscript Received February 3, 2000

ABSTRACT: To terminate transcription in *E. coli*, Rho protein binds an RNA loading site on the nascent transcript, translocates 5′→ 3′ along the RNA in an ATP-driven process, and, upon reaching the transcription elongation complex, brings about RNA release. Thus, the Rho-dependent termination process can be viewed, in part, as a kinetic competition between the rate of transcript elongation by RNA polymerase (RNAP) and the rate of Rho translocation along the nascent transcript. In the context of this model, NusG, which is an essential *E. coli* protein, regulates Rho-dependent termination in an apparently paradoxical way, increasing the rate of transcription elongation of *E. coli* RNAP in the absence of Rho while also shifting the sites of Rho-dependent termination upstream on the template. Here we investigate the regulation of Rho-dependent termination by NusG. Analytical ultracentrifugation was used to establish the existence of a stable complex of NusG and Rho and to demonstrate a stoichiometry of one NusG monomer per Rho hexamer. Surface plasmon resonance was used to examine the kinetics of the formation and dissociation of the NusG−Rho complex, yielding an association rate constant (k_{on}) of 2.8 (±0.8) × 10^5 M^{-1} s^{-1}, a dissociation rate constant (k_{off}) of 3.9 (±0.7) × 10^{-3} s^{-1}, and a calculated equilibrium (dissociation) constant (K_d) of 1.5 (±0.3) × 10^{-8} M. The apparent stability of the NusG−Rho complex is insensitive to changes in salt (potassium acetate) concentration between 0.05 and 0.15 M. The translocation and transcription termination activities of Rho at saturating NusG concentrations were, however, both sensitive to salt concentration over this range, suggesting that these activities do not directly reflect the stability of the NusG−Rho complex. Rho-dependent termination could be demonstrated for transcription complexes in which *E. coli* RNAP had been substituted by either bacteriophage SP6 or T7 RNAP. NusG, however, was not active in transcription termination assays with either of these phage RNAPs. Thus, we conclude that NusG modulates Rho-dependent termination by interacting specifically with the RNAP of the *E. coli* elongation complex to render the complex more susceptible to the termination activity of Rho.

Transcription termination occurs in *E. coli* by two separate pathways. In intrinsic termination, the elongation complex responds directly to transcribed signals on the DNA template. The efficiency of the intrinsic termination process can be modulated by protein regulators, but no additional factors are required to manifest the basic termination response (for a recent review, see *1*). In contrast, Rho-dependent termination requires the function of Rho protein (*2*). Current models typically divide the basic mechanism for Rho function into the following three stages: (i) a Rho hexamer binds to an "unstructured" loading site on the nascent RNA; (ii) Rho translocates, 5′→ 3′, along the RNA transcript in an ATP-driven reaction; and (iii) Rho reaches the transcription elongation complex and triggers release of the RNA transcript (for reviews, see *3*−*6*). These basic models thus suggest that Rho travels along the nascent RNA, "chasing" the elongation complex that is moving in the same direction along the DNA template, and that termination occurs when Rho "catches up with" the elongation complex. In its simplest aspects, this view of Rho action is sometimes called "kinetic coupling" (e.g., see *7*).

The actual mechanism must have additional elements, since it is clear that at some template positions, at which the elongating RNA polymerase (RNAP)[1] pauses for significant lengths of time, Rho does catch up with the elongation complex without bringing about significant termination. This argues that a simple kinetic competition model is not sufficient to explain the termination activity of Rho (*8, 9*). Furthermore, of the three stages of Rho-dependent termination listed above, the details of the last stage (iii) are least well understood, although it is clear that a major component of Rho-dependent transcription termination activity involves the function of Rho as an RNA−DNA helicase to release the nascent RNA from the transcription complex (*10*−*13*).

NusG is an essential *E. coli* protein (*14*) which was originally discovered as an N-dependent antitermination

† This work was supported in part by American Cancer Society Postdoctoral Fellowship PF-98-022-01-MBC to Z.P., by U.S. Public Health Service Research Grants GM15792 and GM29158 to P.H.v.H., and by a Lucille P. Markey Charitable Trust grant to the Institute of Molecular Biology at the University of Oregon. P.H.v.H. is an American Cancer Society Research Professor of Chemistry.

* To whom correspondence should be addressed. E-mail: petevh@molbio.uoregon.edu.

[1] Abbreviations: DTT, dithiothreitol; EDTA, ethylenediaminetetraacetic acid; HEPES, *N*-(2-hydroxyethyl)piperazine-*N*′-2-ethanesulfonic acid; IPTG, isopropyl β-D-thiogalactopyranoside; PCR, polymerase chain reaction; RNAP, RNA polymerase; RU, resonance units; SPR, surface plasmon resonance; Tris, tris(hydroxymethyl)aminomethane.

10.1021/bi992658z CCC: $19.00
Published on Web 04/13/2000

enhancing activity (*15*). NusG alone can accelerate somewhat the rate of elongation of *E. coli* RNA polymerase along the DNA template in vitro and in vivo (*16, 17*). This factor also appears to be required for the function of some Rho-dependent terminators in vivo (*18*) and in vitro (*19*). In addition, NusG can promote Rho-dependent termination at upstream template positions (*20, 21*) as well as at Rho-dependent termination positions observed in the absence of NusG (*19*). It has, however, remained unclear at which stage(s) of the Rho-dependent termination process, and how, NusG acts to stimulate upstream termination.

To investigate these mechanistic issues, we have here examined the interactions of NusG with the other proteins involved in Rho-dependent termination. Utilizing analytical ultracentrifugation, we have demonstrated that Rho and NusG form a stable and specific binary complex with a stoichiometry of one NusG monomer per Rho hexamer. By means of the more sensitive surface plasmon resonance technique, we also have measured the rate constants (k_{on} and k_{off}) for the binding of NusG to the Rho hexamer, and from these parameters have determined a K_d value of 1.5×10^{-8} M for the binary complex. We also have shown that k_{on} and k_{off} are not sensitive to changes in salt concentration (KOAc) between 0.05 and 0.15 M.

To relate these physical findings to the biological activity of NusG, we have analyzed the products of in vitro transcription termination reactions with purified components over the same range of KOAc concentrations, taking advantage of the fact that increasing the concentration of salt over this range results both in slowing the translocation rate of Rho along the transcript and in lowering the apparent processivity of this process (*22*). Quantitative analysis of termination reaction products shows that NusG promotes the upstream shift of Rho-dependent termination over the entire 0.05−0.15 M salt concentration range, but does not overcome the effect of salt on the rate and processivity of the translocation of Rho along the nascent transcript. In addition, we have confirmed (*20*) that NusG does not perturb Rho helicase assays that are performed in the absence of RNAP. Finally, we present experiments with elongation complexes containing either T7 or SP6 RNAP and show that Rho exhibits termination activity with these phage polymerases. Unlike Rho-dependent termination in *E. coli*, however, Rho-dependent termination with the phage polymerases is not perturbed by NusG.

Taken together, these findings show that a specific and stable complex forms between NusG monomers and Rho hexamers during the transcription termination process, but that the functional activity of NusG in this process depends on a direct and specific interaction of NusG with the RNAP. Based on these results and others in the literature, we propose a model describing the effect of NusG on the elongation complex by coupling through a ternary NusG−Rho−RNAP complex.

MATERIALS AND METHODS

Cloning, Expression, and Purification of NusG. Primers for the polymerase chain reaction (PCR) with Pfu DNA polymerase (Stratagene) were designed using *E. coli K12 nusG* sequence information (*14*), forming a genomic DNA template that contains the entire *nusG* protein-coding sequence and the associated translation stop codon. This DNA fragment was cloned into pET11a (Novagen) between the *Nde* I and *Bam*H I sites, creating pET11a/NusG. Inserts in isolated plasmids were sequenced to confirm their accuracy. BL21(DE3) cells were transformed with pET11a/NusG and grown, with shaking, to an OD_{600} of 0.5 in a final volume of 4 L of LB medium with 100 mg/mL ampicilin at 37 °C. IPTG was added to a final concentration of 1 mM, and the cells were grown for an additional 3 h, harvested by centrifugation for 10 min at 5000*g*, and stored at −70 °C.

The transformed cells were resuspended at 10 mL/g in lysis buffer (20 mM Tris-HCl, pH 7.8, 3 mM EDTA, 1 mM DTT, 100 mM NaCl, 20 mg/mL PMSF), lysozyme was added to 0.2 mg/mL, and the cells were incubated for 10 min at 22 °C, and then for 20 min on ice. All of the following steps were performed at 4 °C, unless otherwise noted. Sodium deoxycholate was added to a final concentration of 0.06% (w/v), and the resulting solution was incubated for 20 min. NaCl was added to 0.3 M, and the lysate was sonicated 4 times for 15 s at 22 °C, with 3 min on ice between sonication treatments. Polymin P was added dropwise, with stirring, to a final concentration of 0.6%, after which the lysate was incubated for 20 min and centrifuged at 12000*g*. Ammonium sulfate at 50% of saturation was added to the supernatant dropwise, with stirring, and incubated for 30 min. The lysate was centrifuged for 20 min at 12000*g* and the pellet resuspended in 30 mL of buffer Q (10 mM Tris-HCl, pH 7.8, 1 mM EDTA, 1 mM DTT, 5% glycerol). The lysate was then dialyzed against 4 × 1 L changes of buffer Q for a total of 16 h and spun at 12000*g*, and the supernatant was pumped onto a Q-Sepharose (Pharmacia) column (2.6 cm diameter, 9 cm height) at 13 mL/h. NusG was eluted with a linear 0−200 mM NaCl gradient in buffer Q at 22 mL/h, and 20 μL of each 3 mL fraction were loaded on 15% Laemmli polyacrylamide gels (*23*) and stained with Coomassie Brilliant Blue R-250 (Sigma) after electrophoresis.

Fractions containing NusG were pooled, NaCl was added to 0.5 M, and the solution was chromatographed on a Bio Gel A 5m (BioRad) column (3 cm diameter, 90 cm height) at 25 mL/h. Five milliliter fractions were collected in the same buffer and analyzed as above. Fractions containing pure NusG were pooled, precipitated with ammonium sulfate, resuspended in 10 mL of 20 mM Tris-HCl, pH 7.8, 200 mM NaCl, 0.2 mM EDTA, 0.2 mM DTT, and 5% glycerol, and dialyzed against this buffer as described above. Glycerol was added to 55% to complete the NusG storage buffer, and the protein was stored in 1 mL aliquots at −70 °C or after thawing at −20 °C. The yield of purified NusG protein from 10 g of wet cell pellet was 108 mg.

Analytical Ultracentrifugation. Storage buffers were exchanged, using Biospin P-6 columns (BioRad), for a buffer containing 20 mM Tris-HCl (pH 7.8), 0.1 mM EDTA, 5 mM $Mg(OAc)_2$, 1 mM DTT, and 100 mM KOAc. All the ultracentrifuge runs were conducted at 20 °C in a Beckman model XL-I Analytical Ultracentrifuge with an An-60 Ti rotor, and the progress of the sedimentation process was monitored by light absorption at 229 or 280 nm. Velocity sedimentation experiments were run at 45 000−60 000 rpm for 4−6 h in cells equipped with double-sector centerpieces, using 0.3 mL volumes of protein solution and 0.31 mL of buffer as the reference solution. Sedimentation data were

analyzed after the proteins had cleared the meniscus. Van Holde−Weischet data analysis (*24*) was performed using an Ultrascan 2.0 (gift of B. Demeler, University of Texas, San Antonio) in a Microcal Origin 3.78 program (Beckman). The time-derivative data analysis (*25*) was performed using a Dcdt 60 program (gift of W. Stafford, Boston Biomedical Research Institute). Simulations of velocity sedimentation experiments were carried out using Ultrascan 4.0 (gift of B. Demeler, University of Texas, San Antonio). The Sednterp program (gift of D. Hayes, Magdalen College, T. Laue, University of New Hempshire, and J. Philo, Amgen) was used to calculate the partial specific volume of the proteins, and the viscosity and density of the solutions.

Equilibrium sedimentation experiments were run at 20 °C and 25 000 or 30 000 rpm for 16−24 h in cells equipped with six-channel centerpieces, using 0.10 mL volumes of protein solution and 0.11 mL of buffer in the reference cell. The Match 7.0 program (gift of D. Yphantis, University of Connecticut) was used to establish that equilibrium had been reached in each run. Data were analyzed using the WinNon-Lin 1.06 program (gift of D. Yphantis, M. Johnson, and J. Lary, University of Connecticut). Global analysis of seven or eight different sample concentrations was performed.

Surface Plasmon Resonance. Experiments were performed at 20 °C using a Biacore model X surface plasmon resonance apparatus. The running buffer was identical to that used in the analytical ultracentrifugation experiments, except that the concentration of KOAc was varied between 50 and 150 mM (as described in the text), and 20 mM HEPES (pH 7.9) was used instead of 20 mM Tris-HCl (pH 7.9) because Tris buffers sometimes give erratic signals in the Biacore (D. McMillen, University of Oregon Biotechnology Laboratory, unpublished). All reagents, except for proteins and running buffers, were obtained from Biacore. A total of 500−800 RU of NusG were immobilized on the surfaces of CM5 chips, using NHS (*N*-hydroxysuccinimide)/EDC [*N*-ethyl-*N*′-(3-diethylaminopropyl)carbodiimide] amine coupling chemistry according to the manufacturer's guidelines. Solutions containing Rho hexamers with rC_{85-110} (see below) were introduced into the flow cells at 10, 50, or 80 μL/min, and binding was monitored by changes in the refractive index of the solution near the surface of the chip on which NusG had been immobilized. Regeneration buffers containing 10 mM acetate (pH 5.5) and 0.5 M KOAc were applied to the flow cells for 1 min. Experimental results were fit to a simple 1:1 binding model for the interaction of NusG monomers and Rho hexamers using a nonlinear least-squares algorithm provided by the manufacturer. In each experiment, 3−4 data curves were fit globally. Experiments were repeated 3−4 times.

Size Fractionation of Poly(rC). Solutions (3−4.5 mg/mL) of mixed-length poly(rC) (Pharmacia) were treated with 0.1 M $NaHCO_3$ (pH 10.0) at 90 °C for 10 min, followed by 5 min on ice at the same pH, to produce an appropriate distribution of oligo(rC) fragments of shorter length. Solutions were then brought to neutral pH with concentrated HCl and loaded onto 30 × 20 × 0.1 cm denaturing 15% polyacrylamide/bisacrylamide (1:29), 8 M urea, 1 × Tris−borate−EDTA gels. RNA markers 85 and 110 nt in length containing sequences from the *E. coli trp t*′ gene were prepared by runoff transcription reactions with T7 or SP6 RNA polymerase and loaded beside the poly(rC) RNAs. The RNA samples were subjected to electrophoresis at 50 W for 2 h. Gel slices containing treated poly(rC) fractions that ran between the markers were cut, crushed, and soaked in 10 mM HEPES (pH 7.9) for 20 h at 4 °C. The resulting solution was then chromatographed on a C-18 SEPPAK column (Waters) and eluted with 100% methanol. The RNA oligomers obtained were dried in a speed-vac, resuspended in water, precipitated from ethanol containing 0.3 M NaOAc (pH 7.0), collected by centrifugation at 14000*g* for 20 min, washed with 80% ethanol, dried, resuspended in water, and stored at −80 °C. A 0.62 mg sample of oligo(rC) in this size range (designated rC_{85-110}) was obtained from 50 mg of mixed-length input poly(rC).

RNA Molecular Weight Standards. A plasmid carrying the *trp t*′ terminator downstream of an SP6 or T7 RNA polymerase promoter (*12*) was subjected to restriction enzyme cleavage at several different positions and transcribed in vitro. The resulting promoter-dependent RNA sequences of 85, 118, 133, 151, 166, 196, 243, 255, and 276 nt should be identical to those obtained in the termination reactions. These "calibration RNAs" were resolved using denaturing gels, and the resulting mobilities were plotted against the known molecular weights as a semilog plot (data not shown). The results fit well to a straight line using the KaleidaGraph version 3.0.4 program (correlation coefficient $R^2 = 0.994$), permitting us to use the resulting empirical linear equation ($y = 5.357 - 0.0699x$) to determine the molecular weights of the RNA transcripts produced in the termination reactions.

Transcription Reactions. The *E. coli* RNAP transcription template contained the T7A1 promoter, the *E. coli trp t*′ Rho loading site, and the *trp t*′ terminator region [same as the Pt′ template used by Zhu and von Hippel (*9*)]. SP6 and T7 RNAP templates were constructed using PCR amplification with Pfu DNA polymerase (Stratagene), the appropriate promoter sequences, and downstream sequences identical to the *E. coli* templates. Taq DNA polymerase and dATP were used to add an A residue to each DNA fragment at the 3′-end, and the resulting products were cloned into a pGEM T-easy vector (Promega). Transcription initiation (stalled elongation complex formation) reactions contained 20 mM Tris-HCl (pH 7.8), 0.1 mM EDTA, 5 mM $Mg(OAc)_2$, 1 mM DTT, 5% glycerol, 50 mM KOAc, 20 μM each of ATP, CTP, and GTP (Sigma), 100 μM ApU [adenylyl(3′ → 5′)uridine] (Sigma), 0.15 μM [α-^{32}P]ATP or [α-^{32}P]CTP (NEN, 3000 Ci/mmol), 40 nM DNA template, and 80 nM RNA polymerase. Reactions were incubated for 5 min at 30 °C. The SP6 and T7 RNAPs were from Promega; *E. coli* RNAP holoenzyme was purified by S. Weitzel of our laboratory as described in Burgess and Jendrisak (*26*), except that the Biorex 70 chromatography step was omitted.

Transcription elongation−termination reactions with *E. coli* RNAP contained final concentrations of 20 mM Tris-HCl (pH 7.8), 0.1 mM EDTA, 5 mM $Mg(OAc)_2$, 1 mM DTT, 5% glycerol, 50−150 mM KOAc (as described in the text), 1 mM NTP, 50 μg/mL rifampicin (Sigma), 100 nM Rho hexamers (a generous gift of K. Walstrom of our laboratory, purified as described in *12*) or an equal volume of Rho storage buffer (*12*), and NusG (as described in the text) or an equal volume of NusG storage buffer (described under Cloning, Expression, and Purification of NusG). Elongation−termination reactions with SP6 or T7 RNAP contained final concentrations of 20 mM Tris-HCl (pH 7.8),

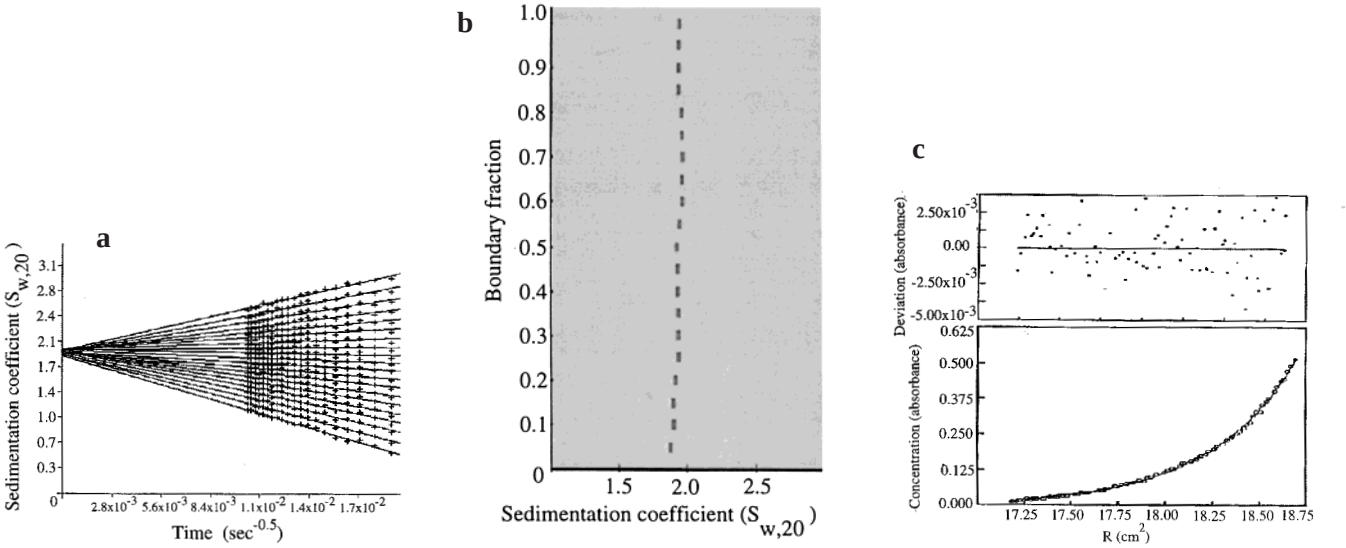

FIGURE 1: Analysis of NusG by analytical ultracentrifugation. (a) Van Holde−Weischet analysis of a velocity sedimentation experiment. A 5 μM solution of NusG was subjected to velocity sedimentation at 52 500 rpm for 6 h, and the sedimentation process was monitored by UV absorbance at 229 nm (see Materials and Methods). The boundary was divided into 20 segments, and the sedimentation coefficient in each segment was calculated. Data were fit using a linear least-squares routine and extrapolating to infinite time. The intercept of each line with the *y*-axis indicates the diffusion-corrected sedimentation coefficient in that part of the boundary. (b) Distribution of the diffusion-corrected sedimentation coefficient along the sedimentation boundary in the velocity sedimentation experiment shown in (a). Because the sedimentation coefficient did not vary along the boundary, this plot is interpreted to indicate that NusG exists as a homogeneous protein with an $s_{w,20}$ of 1.9 S under these conditions. (c) Equilibrium distribution of NusG concentration as a function of distance along the axis of sedimentation. A 10 μM solution of NusG was subjected to equilibrium sedimentation at 30 000 rpm for 20 h, and sedimentation was monitored by light absorption at 280 nm (see Materials and Methods). The circles represent the experimental data, and the solid curve is fitted to a simple monomer model with no higher association states. The residuals representing the deviation of the experimental data from the model curve are shown above the graph along the same *x*-axis; but with a 50-fold expanded y-axis.

0.1 mM EDTA, 5 mM $Mg(OAc)_2$, 1 mM DTT, 5% glycerol, 40 μM each of CTP, GTP, and UTP, 1 mM ATP, 8 mM DNA template trap (see text), 100 nM Rho hexamers or Rho storage buffer, and NusG (as described in the text) or NusG storage buffer. Equal volumes (typically 5 μL) of stalled elongation complexes (described above) and termination mix were combined; reactions were incubated for 5 min at 30 °C and quenched by the addition of an equal volume (10 μL) of loading buffer (85% deionized formamide, 20 mM EDTA, 0.1% bromophenol blue, 0.1% xylene cyanol). Reactions were boiled for 4 min and loaded on denaturing 15% polyacrylamide (1:29 acrylamide/bisacrylamide), 8 M urea, 1 × Tris−borate−EDTA gels.

RESULTS

Analytical Ultracentrifugation of NusG−Rho Complexes. Binding interactions between Rho and NusG were initially detected by an affinity chromatography approach in which a crude *E. coli* extract was applied to a column of tethered NusG. Rho was the only protein bound in detectable quantities (*27*). Since this interaction might be crucial to the role of NusG in Rho-dependent termination, we have characterized it further. We first used analytical ultracentrifugation to confirm the physical parameters of Rho that had been previously described by Geiselmann et al. (*28, 29*).

Velocity sedimentation experiments were analyzed by the Van Holde−Weischet (*24*) and time derivative methods (*25*). At 20 °C and in Rho concentrations (in Rho monomer units) of 10−20 μM, in buffer containing 20 mM Tris-HCl (pH 7.8), 0.1 mM EDTA, 5 mM $Mg(OAc)_2$, 1 mM DTT, and 100 mM KOAc, Rho forms a homogeneous solution characterized by a sedimentation coefficient of 10.3 S (data not shown). This value is consistent with the sedimentation constant of 10.2 (±0.2) S measured previously by Geiselmann et al. (*28*) under similar buffer and temperature conditions. This good agreement with previous measurements is significant, because many of the earlier physical chemical Rho studies from this laboratory had been performed with a Rho overexpression protein that was subsequently found to carry an E155K mutation (*30*), whereas the present studies were performed with protein expressed from the wild-type sequence. Thus, this finding can be added to previous measurements that have shown that most (though not all) of the physical properties and enzymic activities of Rho are identical for the wild-type and mutant proteins (*30* and K. Walstrom, J. Dozono, and P. H. von Hippel, manuscript in preparation).

To investigate the solution properties of NusG, sedimentation velocity experiments were performed on a pure protein preparation under the same buffer and temperature conditions used in the experiments with Rho alone. A representative Van Holde−Weischet analysis (*24*) of these NusG data is presented in Figure 1a. This method of analysis is useful because it eliminates the effect of diffusion on the boundary by extrapolating the apparent sedimentation data measured on each section of the boundary to infinite time (this works because diffusion-driven transport rates vary in proportion to $t^{1/2}$, while sedimentation transport rates are directly proportional to t).

In the Van Holde−Weischet method, the sedimenting boundary is typically divided into 20−70 segments, and the *y*-axis intercept of a least-squares linear fit to the apparent sedimentation coefficient of each boundary segment yields the diffusion-corrected sedimentation coefficient for that boundary segment. Convergence of the extrapolated lines for the various segments to a single value near the *y*-axis is

diagnostic of a homogeneous solution, because such a sample should yield the same sedimentation coefficient as a function of time in all parts of the boundary (*31*). Figure 1b shows the distribution of the diffusion-corrected values of $s_{w,20}$ across the sedimenting boundary. Figures 1a and 1b strongly argue that NusG forms a homogeneous solution, as judged by the distribution plot. Analysis of 12 samples of NusG, ranging in (monomer) concentration from 4 to 18 μM and run at rotor speeds of 45 000−60 000 rpm, showed that under these conditions NusG sediments with an $s_{w,20}$ of 1.9 (±0.1) S. The absence of a dependence of the apparent sedimentation coefficient on the concentration of NusG shows that nonideality contributions are negligible for NusG in this protein concentration range.

Equilibrium sedimentation experiments were performed (see Materials and Methods) to further analyze the solution properties of NusG. The data obtained were analyzed using the WinNonLin 1.06 program, and representative results are shown in Figure 1c. The residuals calculated as a function of position in the ultracentrifuge cell are shown above the data and demonstrate that the deviations between the experimental data and the monomer model were small and random, arguing that a simple monomer model fits the data well. Six to seven different NusG samples at (monomer) concentrations ranging from 4 to 18 μM were fit globally to yield a weight-average molecular weight (M_w) of 20 700. The molecular weight calculated from the amino acid sequence is 20 532. We conclude that NusG behaves as a monomer and shows no evidence of higher association states under the conditions examined.

As indicated above, the existence of a complex between NusG and Rho had been inferred earlier by affinity column chromatography (*27*). Sedimentation velocity experiments were performed using mixtures of the two proteins to characterize this binary complex. Because the sedimentation coefficients of the Rho hexamer and the NusG monomer are very different (10.2 S versus 1.9 S), we expected that any unbound NusG could easily be resolved from a putative NusG−Rho complex. Figure 2 shows that two clear boundaries form relatively early in sedimentation velocity experiments with Rho−NusG mixtures, as predicted by the difference in the sedimentation coefficients of the two species, with the faster sedimenting component almost reaching the bottom of the cell before the slower component had completely cleared the meniscus. By comparing the input concentrations of NusG and Rho to the amounts of protein present in the fast and slow sedimenting components, we showed that the fast component contained more protein than could be accounted for by the input Rho, while the slow component contained less protein than the input NusG. These observations are summarized quantitatively in Table 1.

These results are best fit by a model involving the binding of a single NusG monomer to a Rho hexamer. We note that when Rho forms higher order association states, for example, at concentrations higher than 5 μM hexamer (*28*), we no longer observe the binding of NusG to that Rho fraction, suggesting that NusG binding is specific and the formation of Rho association states higher than hexamers obscures the NusG binding site on the hexamer. We conclude that the binding stoichiometry data extracted from these velocity sedimentation experiments are best fit by a 1:6 complex of NusG-Rho monomers.

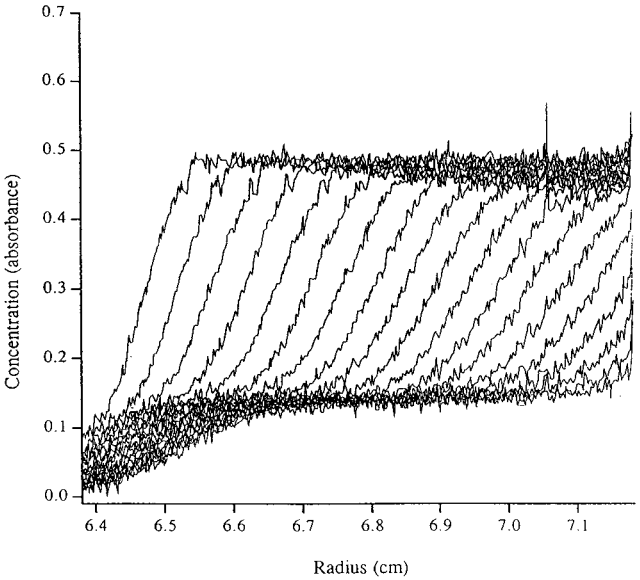

FIGURE 2: Velocity sedimentation of Rho and NusG. A solution of 9.4 μM NusG and 17.1 μM Rho (concentrations in monomers) was subjected to velocity sedimentation at 52 500 rpm for 6 h (see Materials and Methods). Sedimentation was monitored by absorbance at 280 nm. Nineteen scans taken in the first hour of the run are shown. The faster-sedimenting component contained ~0.4 absorbance unit of Rho and Rho−NusG complexes. The slower-sedimenting component contained ~0.1 absorbance unit of free NusG.

Table 1: Monomeric NusG and Hexameric Rho Form a Complex

Rho (μM hexamers)	$NusG_{(bound)}$ (μM monomers)[a]	$NusG_{(bound)}$ (μM monomers)[b]
2.4	2.0	2.6
2.8	2.0	2.5
5.1	5.0	5.0

[a] Measured as $NusG_{(total)} - NusG_{(free)}$, where $NusG_{(total)}$ is the total amount of NusG present in the analytical ultracentrifuge cell (measured in a different cell containing no Rho in the same experiment), and $NusG_{(free)}$ is the slower sedimenting component in the cell containing Rho and NusG. [b] Measured as $Rho-NusG_{(complex)} - Rho_{(total)}$, and expressed in terms of NusG monomers, where $Rho-NusG_{(complex)}$ is the amount of protein in the faster sedimenting component in the analytical ultracentrifuge cell centaining both proteins, and $Rho_{(total)}$ is the amount of Rho present in the cell (measured in a different cell contaning no NusG in the same experiment).

We show that the binding of NusG to the Rho hexamers is saturated under the solution conditions used in these sedimentation experiments. As a consequence, these results can only be used to establish an upper limit (10^{-6} M) for the equilibrium dissociation constant (K_d) for the NusG−Rho hexamer complex (the Rho hexamers themselves do not dissociate under these concentration conditions, *28*). The absorbance and interference optical systems of the Beckman XL-I analytical ultracentrifuge cannot be used reliably to measure the distributions of proteins of the sizes of NusG and Rho at concentrations below ~100 nM. Therefore, this method could not be used to determine an actual K_d for the Rho−NusG complex. In addition, because the sedimentation coefficients of Rho hexamer and the NusG−Rho hexamer complex are very similar, the boundaries representing these two components cannot be resolved. Sedimentation velocity simulation procedures (see Materials and Methods) were used to model sedimentation distributions of NusG, Rho hexamers, and NusG−Rho hexamer complexes (data not shown). These

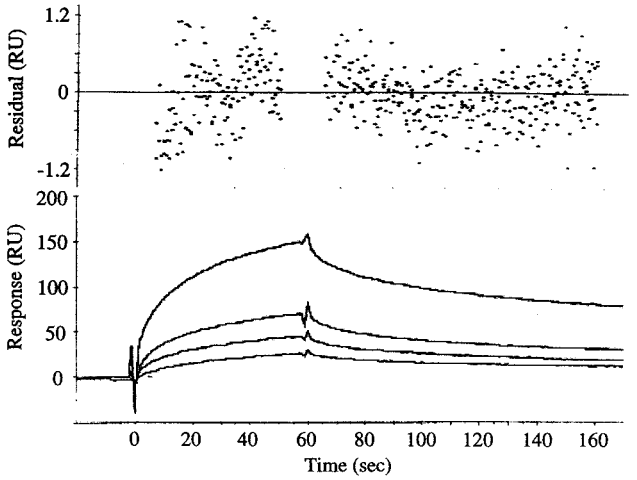

FIGURE 3: Kinetics of Rho−NusG complex formation and dissociation. SPR was used to analyze the interaction between Rho hexamers and NusG. NusG was immobilized to the surface of the chip in the flow chamber (see Materials and Methods). Solutions containing 62, 32, 16, and 8 nM Rho hexamers stabilized by rC_{85-110} were introduced into the binding chamber at 50 μL/min, as described in the text. The data were fit to a 1:1 binding isotherm between Rho hexamers and NusG, and the residuals for the fit are shown above the data. The residuals fall within the error of the detector (1−2 RU) and are randomly distributed in the association and dissociation phases of the experiment.

simulations showed that NusG and Rho hexamers can be resolved easily into two distinct boundaries, regardless of assumptions regarding the gross molecular shapes of the components (sphere, prolate elipsoid, oblate elipsoid, and long rod). These simulations also confirmed that Rho hexamers and NusG−Rho hexamer complexes of any molecular shape cannot be resolved into two species using sedimentation velocity experiments.

SPR Measurements of the Rate Constants for NusG−Rho Complex Formation and Dissociation. Surface plasmon resonance (SPR) methods can be utilized to detect fast changes in the refractive indices of many solutions at relatively low protein concentrations (*32*). Because the refractive index of a solution changes dramatically upon the addition of macromolecules (proteins or nucleic acids), SPR can be a useful tool for the determination of binding kinetics between defined macromolecular components (reviewed in *33*). Here we use these methods to further examine complex formation between NusG and Rho.

NusG was immobilized to the surface of a chip as described under Materials and Methods, and control chips received the same treatment except that NusG was omitted. Solutions containing Rho were then introduced into the flow cell, and binding was monitored by detecting changes in the solution refractive index near the surface of the chip to which NusG had been immobilized. Since Rho hexamers can dissociate partially at low protein concentrations (*28*), poly(rC) was added to the Rho solutions at 5−6-fold molar excess over the Rho hexamer concentrations to maintain Rho in a hexameric state under the conditions used (*34*). To ensure that only one Rho hexamer was bound per RNA chain, we prepared oligomers of poly(rC) that were 85−110 nucleotide residues in length (rC_{85-110}; see Materials and Methods).

A typical SPR experiment is shown in Figure 3, where the amount of Rho bound to the immobilized NusG is plotted against time. In the association part of the experiment (from 0 to 60 s), Rho hexamers were flowed over the chip and binding was monitored as an increase in the refractive index of the solution near the surface. After 60 s, the flow of Rho hexamers was stopped, and buffer was flowed over the chip surface. The dissociation of the NusG−Rho complexes was monitored as a decrease in the refractive index of the solution near the surfaces in the 60−180 s time window. The binding and dissociation curves for several Rho hexamer concentrations were aligned with respect to the time and response axes. Control reactions showed less than 3% of the response obtained with NusG-containing reactions. We attribute these small background signals to nonspecific binding of Rho hexamers to the surface of the chip, and these values were subtracted from the signals obtained with NusG-containing solutions before analysis.

Table 2: Kinetics of Rho−NusG Complex Formation[a]

[KOAc] (M)	k_{on} (M^{-1} s^{-1})	k_{off} (s^{-1})	K_d (M)
0.05	$(2.4 \pm 0.5) \times 10^5$	$(3.2 \pm 0.2) \times 10^{-3}$	$(1.4 \pm 0.3) \times 10^{-8}$
0.10	$(2.6 \pm 0.3) \times 10^5$	$(4.1 \pm 0.8) \times 10^{-3}$	$(1.6 \pm 0.2) \times 10^{-8}$
0.15	$(3.4 \pm 1.0) \times 10^5$	$(4.3 \pm 0.2) \times 10^{-3}$	$(1.4 \pm 0.3) \times 10^{-8}$

[a] Measurements (as described in the text) were repeated 3 times, the average value is reported, and the error is the standard deviation.

The results were fit to a simple 1:1 binding isotherm for the interaction of NusG monomers and Rho hexamers. A nonlinear least-squares fitting algorithm provided by the manufacturer was used to fit the data globally within each experiment. The residual plot of one such fit is shown in Figure 3. Because the noise in the data was 1−2 RU, these residuals fall well within the range of a reasonable fit. Moreover, the residuals were randomly distributed relative to the time course of the experiment, and the χ^2 values (which in these experiments simplify to the sum of the residuals squared per data point) were consistently lower than 0.3. We conclude that a simple 1:1 binding interaction between NusG monomers and Rho hexamers provides a good fit to the data. Measurements were repeated 3−4 times in solutions with a KOAc concentrations of 0.05, 0.10, and 0.15 M. The rate (k_{on} and k_{off}) and equilibrium (K_d) constants obtained are listed in Table 2. For all three salt concentration regimes tested, we obtained k_{on} values of $\sim 10^5$ M^{-1} s^{-1} and k_{off} values of $\sim 10^{-3}$ s^{-1}, yielding calculated K_d values of $\sim 1.5 \times 10^{-8}$ M.

SPR detectors, which have been developed relatively recently, are becoming increasingly popular tools for the analysis of macromolecular interactions in solution. Consequently, attention has been given to the issue of how well the data-fitting models describe the real binding situation (*35*). In our system, Rho hexamers are flowed continuously over the immobilized NusG. Therefore, for each Rho hexamer concentration, the amount of Rho in the flow cell at any time is assumed to be constant. One potential problem with this assumption is that if the concentration of Rho hexamers in the solution layers located closest to NusG is depleted faster than it can be replenished by the flow of new Rho, the concentration of free Rho hexamers that is available for binding within the NusG layer is effectively lowered. To address this issue (which has been termed the mass transport problem), the flow rate of Rho was varied from 10 to 80 μL/min. The results obtained showed that the

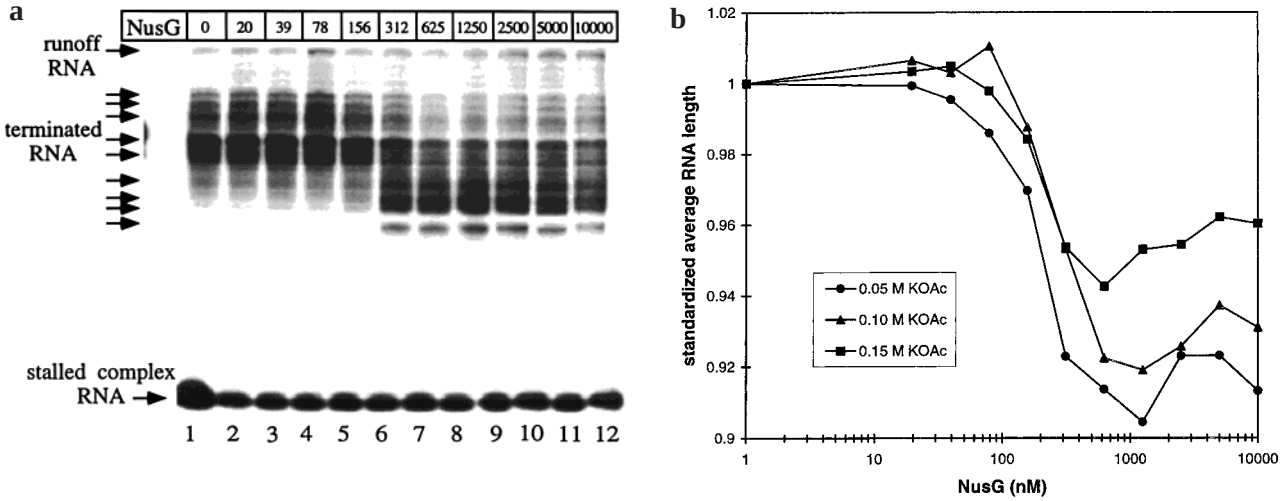

FIGURE 4: NusG promotes upstream Rho-dependent transcription termination. (a) Transcription termination assays. Stalled elongation complexes (lane 1) were prepared as described in the text. Single-turnover elongation reactions were performed with Rho (lane 2) and with Rho in the presence of increasing concentrations of NusG (lanes 3−12). NusG concentrations (in nM) are shown above the lanes. Reactions were quenched, and RNAs were resolved on denaturing 15% acrylamide/bisacrylamide gels. Positions of runoff, terminated, and stalled RNAs are indicated at the left of the gel. (b) Quantification of NusG activity. Using RNA standards (see Materials and Methods), weighted average RNA lengths (ARLs) were calculated as described in the text. The concentration of KOAc in the elongation reactions was varied from 0.05 to 0.15 M, and results for each salt condition, as indicated in the graph, are shown as a plot of the ARL against NusG concentration. Experiments at each salt concentration were repeated 3−5 times, and the averages are shown. The standard deviation for each data point was between 1% and 3% of the value plotted.

observed binding kinetics were not sensitive to the flow rate of the Rho solution (data not shown), arguing that the results are not perturbed by mass transport effects and that the concentrations of free Rho hexamers in solution can indeed be treated as constant in each experiment.[2]

The K_d values obtained from apparent rate constants measured by SPR are consistent with limit values of this parameter estimated from sedimentation velocity experiments performed under similar conditions, but at higher protein concentrations and without rC_{85-110}, which placed an upper limit of $\sim 10^{-6}$ M on the K_d for the NusG−Rho complex. Moreover, even if the SPR technique suffers from systematic errors that we have yet to uncover, the comparison of binding rates under different salt conditions is certainly valid, and these data argue strongly that the interaction of NusG with Rho hexamers is constant for salt concentrations between 0.05 and 0.15 M KOAc.

[2] SPR detection is particularly well-suited for measuring macromolecular kinetic binding parameters, but is less ideal for the direct determination of equilibrium constants, which are typically derived from the ratios of the observed k_{on} and k_{off} values. To check this procedure, Myszka and colleagues compared equilibrium binding constants derived from the kinetic constants of three systems analyzed by SPR technology to the equilibrium binding constants obtained directly by isothermal titration microcalorimetry (ITC). Yoo et al. (*36*) studied the interaction of the 16 kDa monomeric HIV capsid protein (CA) fragment with the 18 kDa human cyclophilin A (CypA). A K_d value of 16 (±4) μM was obtained for the monomer−monomer binding interaction using ITC, in good agreement with a K_d of 18 (±2) μM calculated from k_{on} and k_{off} data using SPR. In a second set of experiments, Myszka et al. (*37*) analyzed the interaction of an ~45 kDa soluble truncated human CD4 receptor with an anti-CD4 monoclonal antibody. A K_d of 0.2 (±0.1) nM was obtained using ITC, in good accord with the K_d of 0.24 (±0.01) nM calculated using SPR data. Finally, Joss et al. (*38*) analyzed the binding interaction of an ~52 kDa Fab fragment of anti-CD4 antibody with a mutated and soluble truncated CD4 receptor. A K_d of 2.6 (±0.5) nM was obtained by ITC, in good agreement with the K_d value obtained by SPR of 2.20 (±0.01) nM. These data suggest that K_d data obtained by SPR can, despite some experimental limitations, be compared directly to those obtained by standard "thermodynamic" methods.

NusG Shifts Rho-Dependent Termination to Upstream Template Positions. To determine the effects of NusG on Rho-dependent termination, we performed in vitro single-turnover Rho-dependent termination reactions as a function of NusG concentration, using the well-characterized *E. coli trp t′* termplate as our assay system (*9, 20, 21, 39*). Elongation complexes stalled at template position +29 were prepared by omitting UTP from the initiation reaction (*40*), and were then "chased" with all four required NTPs in the presence of Rho and increasing amounts of NusG (see Materials and Methods). In agreement with previous findings (*9, 20, 21, 39*), Rho-dependent termination on this template occurs over a range of about 100 nts (Figure 4a, lane 2). In addition, NusG caused an upstream shift in the template positions at which Rho-induced termination occurred (Figure 4a, lanes 3−12). In the absence of NusG, Rho-dependent termination at these upstream positions was not detected.

To permit a quantitative determination of the effect of NusG on the Rho-dependent termination reaction, we measured the lengths of the RNA chains formed during this reaction. For this purpose, the gel mobilities of the product RNAs were calibrated against RNA molecular weight standards (see Materials and Methods). The region of the gel containing the terminated RNAs was divided into 10 fractions, and the average length of the RNA chains included in each fraction was calculated. A Phosphorimager was used to determine the amount of RNA in each fraction. Finally, a weighted average RNA length (ARL) was calculated for each termination reaction using the formula:

$$\mathrm{ARL} = \sum_i \mathrm{RNA}_{\mathrm{amount}} \times \sum_i \mathrm{RNA}_{\mathrm{length}} / \sum_i \mathrm{RNA}_{\mathrm{amount}} \quad (1)$$

with each sum taken over all (i) fractions of the gel. For each experiment, the ARL value was set to unity in reactions containing Rho but no NusG, and the ARL for each reaction containing both NusG and Rho was expressed as a fraction.

This analysis was applied to experiments such as that shown in Figure 4a, yielding results such as those shown in Figure 4b. Increasing the amounts of NusG in the reaction decreased the apparent ARL over the 80−800 nM NusG concentration range. Further increases in NusG concentration (to 1.25−5.00 μM) reversed this trend and resulted in a slight, but reproducible, increase in average transcript length.

Effects of Changes in Salt Concentration. As the concentration of KOAc was increased from 0.05 to 0.15 M, the overall Rho-dependent termination efficiency was decreased (data not shown), in agreement with previous results (*11*). The range of NusG concentrations at which NusG-dependent effects on termination positions were most pronounced (Figure 4b, 80−800 nM) did not vary markedly as the salt concentration was increased. These results are consistent with our finding that formation of the Rho−NusG complex is not sensitive to changes in KOAc concentration between 0.05 and 0.15 M (Table 2), and argue that similar levels of this complex were formed during the termination reaction across this entire salt concentration range. In addition, at NusG concentrations over 1 μM, the ARL values obtained at different salt concentrations did not converge, but instead remained at distinct levels.

At these NusG concentrations, based on a K_d value of $\sim 1.5 \times 10^{-8}$ M for the NusG−Rho complex (Table 2), all the Rho hexamers present should be bound by NusG. Therefore, these data suggest that at saturating levels of NusG the effect of increasing salt concentrations on Rho-dependent termination cannot be overcome by increasing the NusG concentration further. Increasing salt concentration results in lowered affinities of Rho for the RNA, as well as lowered translocation rates and processivities (*12, 13, 22*). A model that is consistent with these results posits that NusG does not affect those stages of the termination reaction that involve the binding of Rho to, and its translocation along, the RNA lattice. Instead NusG activity can be reconciled with the effects of salt concentration if NusG acts at a different stage in the termination reaction, i.e., at the step(s) involved in the interaction of Rho with the RNA polymerase of the transcription elongation complex (see Discussion).

Rho and NusG Activities with Elongation Complexes Formed with Bacteriophage SP6 and T7 RNA Polymerases. We have shown that Rho hexamers [stabilized by poly(rC)] form stable and specific complexes with NusG over the 0.05−0.15 M salt concentration range (Figures 2 and 3, Tables 1 and 2), and that NusG is active at all three salt concentrations tested in this range (Figure 4b). We have also shown that the observed efficiency of Rho-dependent transcription termination decreases with increasing salt concentration over this range and that the addition of NusG cannot overcome this salt concentration-dependent effect. Since Rho and NusG are apparently bound as stable complexes at termination reactions in all three salt concentration regimes examined, we asked whether the effect of NusG on Rho-dependent transcription termination is manifested at the point of the interaction of Rho with the elongating RNAP.

To this end we substituted *E. coli* RNAP with either phage T7 or SP6 RNAP in the Rho-dependent transcription termination reaction. The rationale for these experiments was that if Rho were active in transcription termination with these RNAPs, we could ask whether NusG enhances this Rho activity with the phage polymerases. Thus, if NusG was found to be active in Rho-dependent termination with SP6 or T7 RNAP, this would argue that the NusG interaction is not RNAP-specific. If NusG was found not to be active in Rho-dependent termination with the phage RNAPs, this result would argue that NusG activity depends on the interaction of NusG (and Rho) with *E. coli* RNAP. A change in NusG activity of this sort would also argue that a ternary interaction of NusG with Rho and *E. coli* RNAP is essential for the upstream-shift of Rho-dependent transcription termination.

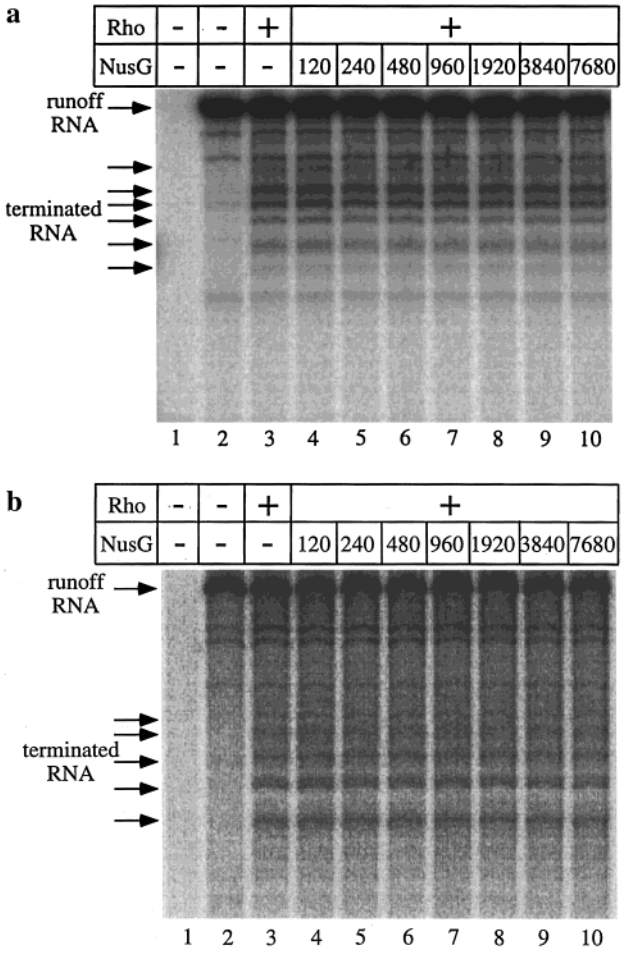

FIGURE 5: Rho-dependent termination with transcription complexes containing SP6 or T7 RNAP is not affected by NusG. (a) Transcription termination reactions with SP6 RNA polymerase. Stalled transcription complexes were formed as in Figure 4. Reactions were quenched (lane 1), or chased with no additional protein factors (lane 2), or in the presence of Rho (lane 3), or in the presence of Rho and NusG (lanes 4−10). NusG concentrations (nM) are indicated above each lane. The positions of the runoff RNA and of the Rho-terminated RNAs are indicated to the left of the gel. (b) Transcription termination reactions with T7 RNA polymerase. Experimental conditions and lanes were the same as in Figure 5a.

To conduct this test, we performed transcription termination experiments similar to those shown in Figure 4, except that SP6 or T7 RNAP was substituted for *E. coli* RNAP. The templates for the experiments with the phage RNAPs were identical to those used in the experiments with *E. coli* RNAP, except that appropriate phage promoter sequences were substituted upstream of the transcription start site. Multiple turnover termination reactions with SP6 and T7 RNAPs are shown in Figure 5a and 5b, respectively. These experiments demonstrated that Rho can bring about transcription termination with both phage polymerases (compare

Table 3: Efficiency of Rho-Dependent Termination with *E. coli*, SP6, and T7 RNA Polymerases

RNA polymerase	termination efficiency[a]
E. coli	1.67 ± 0.08
SP6	1.31 ± 0.08
T7	1.03 ± 0.01

[a] Termination efficiency was determined in single-turnover reactions and is given by: $(RNA_{term(+)Rho} \times RNA_{total(-)Rho})/(RNA_{total(+)Rho} \times RNA_{term(-)Rho})$, where RNA_{term} is the amount of terminated RNA, RNA_{total} is the sum of runoff and terminated RNA, and $_{(-)Rho}$ or $_{(+)Rho}$ denotes reactions in the absence or presence of Rho, respectively (also see Materials and Methods). A termination efficiency value of 1.00 represents no termination activity, whereas infinity would indicate complete activity. Measurements were repeated 3−6 times, and the error given is the standard deviation.

lanes 2 and 3), although with different efficiencies. We note that the effect of Rho on termination with T7 RNAP is small (also see Table 3), but clearly and reproducibly detectable.

To compare the *E. coli* and the phage RNAPs under similar reaction conditions, single-turnover reaction conditions had to be devised for the reactions conducted with the SP6 and T7 RNAPs (see also Materials and Methods). A double-stranded DNA trap containing the appropriate promoter sequence and a short template sequence to be transcribed was included in the chase phase of the experiment at 400-fold excess over the concentration of the long template. As a consequence, all the RNAPs should be trapped on the short template after one round of transcription on the long template. An additional consideration is that the average elongation rate of T7 and SP6 RNAPs is 4−10 times larger than that of *E. coli* RNAP (*41, 42*). To obtain comparable average elongation rates, we lowered the rates of the phage RNAPs by decreasing the concentration of CTP, GTP, and UTP in the elongation phase from 1 mM to 40 μM (the concentration of ATP was held at 1 mM to maintain the same rate of Rho translocation along the transcript with all the RNAPs tested). We note that even at NTP concentrations of 1 mM, the Rho dependence of the termination activity with SP6 and T7 RNAPs was maintained, arguing that even at higher elongation rates Rho was able to "catch-up-with" these RNAPs.

As predicted, inclusion of the trap template in the initiation phase of the experiment abolished transcription from the experimental (long) template, and inclusion of the trap template in the elongation phase of the experiment resulted in transcription of the trap sequence (data not shown). In addition, the amount of RNA transcribed from the experimental template was decreased dramatically in the presence of the trap template (data not shown). Table 3 provides the quantification for single-turnover termination reactions containing Rho and different RNA polymerases. Rho termination activity was most robust with *E. coli* RNAP, intermediate with SP6 RNAP, and weakest with T7 RNAP.

Figures 5a and 5b show the result of adding NusG to Rho-dependent termination reactions with the phage RNAPs (lanes 4−10). These results show that NusG does not enhance the activity of Rho with these RNAPs. The same NusG preparation, however, was active with *E. coli* RNAP (Figure 4). Because the only component of the reaction that was changed in these experiments was RNAP, these findings strongly support a model in which NusG acts to modify the interaction of Rho with *E. coli* RNAP, but not the interaction of Rho with either SP6 or T7 RNAP.

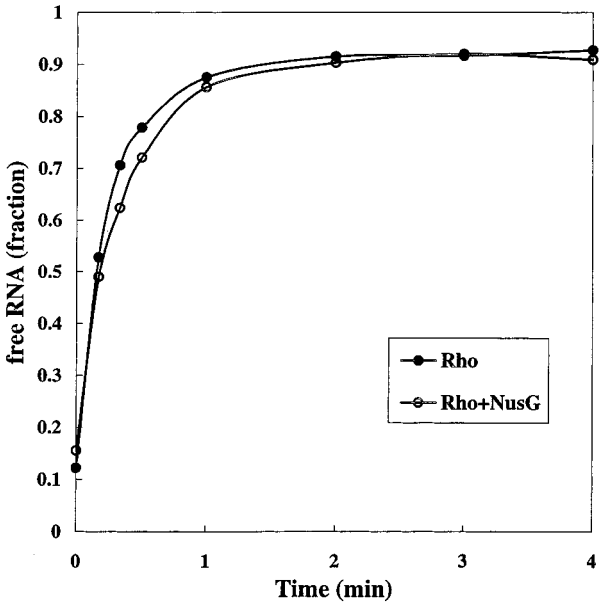

FIGURE 6: Rho helicase activity is not enhanced by NusG. Single-turnover Rho-dependent helicase assays of an RNA−DNA duplex were performed (*12*), and the fraction of free RNA present is plotted as a function of time. Experiments containing Rho alone or Rho and NusG were repeated 3 times, and the average values are reported. The standard deviation of each data point was 1−5% of the plotted value.

The Helicase Activity of Rho Is Unaffected by NusG. While the above results certainly suggest that the NusG effect is specific to the *E. coli* RNAP, it remained possible that NusG acts to increase the efficiency with which Rho works as an RNA−DNA helicase. To test this possibility directly, we performed Rho-dependent helicase assays in the presence and absence of NusG. In these assays, an isolated RNA transcript containing a Rho loading site and the relevant downstream sequences was annealed to a DNA oligonucleotide at the 3′-end of the RNA (*10, 12, 13, 20*). Rho was then bound at the RNA loading site and, in the presence of ATP, translocated 5′→ 3′ and unwound the RNA−DNA duplex at the 3′-end of the RNA. The same *trp t′* RNA that was used for these assays also was transcribed in the Rho-dependent termination reactions detailed above. Our experiments were done under single-turnover conditions and with equivalent molar ratios of Rho hexamers and helicase substrate (*12, 13*).

The rationale for these experiments was that, in principle, if NusG affected Rho RNA binding, Rho translocation, Rho ATPase, Rho-dependent RNA−DNA hybrid unwinding, or any other activity that is independent of RNAP, this effect would be observed as a NusG-dependent effect in the helicase assay. In contrast, if NusG activity in the termination assays depended on specific interactions with *E. coli* RNAP, there should be no NusG effect in Rho helicase assays because here no RNAP is present.

Results of such single-turnover helicase assays with Rho or with Rho and NusG are shown in Figure 6. We found that the rate and amplitude of the reaction were not changed by the presence of NusG. In addition, varying the temperature of the helicase reactions between 20 and 37 °C, and the ATP concentration from 0.1 to 1.0 M, showed no effect of NusG on the helicase activity of Rho. These results are similar to those of Nehrke et al. (*20*), although their helicase experi-

ments were performed under multiple-turnover conditions with a molar excess of Rho over substrate. In addition, Nehrke et al. used different substrates and salt conditions from the ones used here. Their findings and ours are consistent with the conclusion that the binding of NusG to Rho hexamers does not affect the binding of Rho to RNA, nor does NusG binding perturb the ATPase activity, translocation rate, translocation processivity, or RNA−DNA unwinding activities of Rho. Rather, these results strengthen our conclusion that NusG activity is specific to the ternary interaction with the *E. coli* RNAP. A model that can account for all these results posits that NusG expresses its effects on Rho-dependent transcription termination within the step or steps at which Rho interacts with the *E. coli* RNAP in the elongation complex.

DISCUSSION

Physical Characterization of the NusG−Rho Complex. Here we have examined the physical properties of NusG and the complex that it forms with transcription termination factor Rho. We have shown that NusG alone exists as a monomer over a wide range of protein concentrations and that it forms a stable and specific 1:1 complex with the Rho hexamer. The affinity of NusG for the Rho hexamer is relatively high, with $K_d \sim 1.5 \times 10^{-8}$ M for the interaction. Furthermore, as summarized in Table 2, changing the salt concentration (KOAc) from 0.05 to 0.15 M affects neither k_{on} nor k_{off} (nor, by definition, K_d), arguing also that the NusG−Rho interaction is largely nonelectrostatic and specific. Extrapolating from our current findings and earlier physical biochemical studies of Rho structure and assembly (*28*, *29*, *34*), we also conclude that the NusG−Rho complex remains stable and specific when the Rho hexamer interacts with rC_{85-110}, natural RNA, and ATP.

Functional Characterization of the Action of NusG in Rho-Dependent Termination. We have quantitated the activity of NusG in Rho-dependent transcription termination reactions by determining the weighted average length of the transcripts produced in the presence and absence of NusG. These average lengths were determined over the same salt concentration range used in the binding measurements. Qualitatively, we observed that as the salt concentration was increased, the efficiency of Rho-dependent termination was decreased, in agreement with previous findings (*11*). This is expected because the processivity and rate of Rho tracking 5′ → 3′ along the RNA decrease with increasing concentrations of monovalent salt (*22*). Quantitative analysis of the terminated RNAs formed during transcription showed that NusG does not change this effect of increased salt on Rho termination activity (Figure 4b). These results suggest that NusG, although bound to Rho throughout the termination reaction, does not perturb the movement of the Rho hexamer along the nascent transcript. Results of Rho helicase assays (Figure 6) are consistent with this conclusion and further argue that all the other aspects of Rho helicase activity, including RNA binding, ATPase rates, processivity, translocation rate, and the process of RNA−DNA hybrid separation, are unaffected by NusG.

These findings are consistent with those of others (*20*, *21*, *27*, *43*), who have pointed out that the addition of NusG does not significantly change the stability of the complex formed between Rho and RNA, the RNA-dependent ATPase activity of Rho, or the Rho helicase activity. These results led these groups, and well as Washburn et al. (*44*), to suggest that NusG must act at a different stage of the termination reaction. Burns et al. (*43*) indeed have argued that NusG activity in Rho-dependent termination reflects a direct interaction between NusG and *E. coli* RNAP.

Models for the Action of NusG on Rho-Dependent Transcript Termination. We have performed transcript elongation and termination reactions with SP6 and T7 RNA polymerases, and have shown that Rho is active in transcript termination with these RNAPs (Figure 5a,b). Importantly, and in contrast to its activity with *E. coli* RNAP, we have also shown that the addition of NusG does not perturb Rho-dependent termination for the phage elongation complexes. Since the RNAP is the only component that was changed in these reactions, the simplest interpretation of these results is that NusG activity is specific to elongation complexes containing *E. coli* RNAP. Our results can be fully explained by a model in which the NusG−Rho hexamer complex translocates along the RNA as a stable complex, with NusG having no effect on these stages of the Rho-dependent termination reaction. When the Rho−NusG complex reaches the *E. coli* elongation complex, NusG acts to help Rho release the nascent RNA from elongation complexes on which Rho alone cannot act effectively. This interpretation is supported by the fact that NusG (in the absence of Rho) accelerates the rate of *E. coli* RNAP elongation by around 20% (*16*, *17*), a finding that is most easily explained by a direct interaction between NusG and the *E. coli* RNAP.

Li et al. (*27*) have previously suggested, on the basis of affinity chromatography experiments, that NusG forms a weak complex with *E. coli* RNAP. Thus, we can postulate that this putative weak affinity of NusG for *E. coli* RNAP is strengthened by the much higher affinity of NusG for Rho, and the stable NusG−Rho−RNA complex serves to carry NusG to (and tether it at) its functional target, the elongation complex. This may help to stabilize the NusG−RNAP interaction, perhaps in part by increasing the local concentration of NusG at the elongation complex, and may constrain the geometry of the interaction of NusG with RNAP within the ternary complex when Rho is present.

Other data support a slightly different model, in which NusG forms a stable interaction with the elongation complex in the absence of Rho (*17*). In this view, the activity of NusG in Rho-dependent termination remains specific to the *E. coli* elongation complex, but NusG need not be "carried" by Rho to the elongation complex. This model is supported by the finding that the half-maximal saturation of the elongation−stimulation activity of NusG (in the absence of Rho) is achieved at NusG concentrations of ∼12 nM (*17*). Thus, the presumed NusG−elongation complex interaction, which previously (*27*) had been considered to be weak, may in fact be comparable in binding affinity to the interaction between NusG and Rho.

The simplest version of this model is less attractive in light of the present study, since it includes no role for the specific NusG−Rho complex that we have described here. Perhaps a compromise position is that NusG may interact with Rho and RNAP separately with comparable affinities, but the formation of the ternary complex further stabilizes and

constrains interactions within the resulting-Rho-dependent termination complex, making Rho-dependent termination more efficient and shifting it toward upstream sites along the template. A final resolution of these issues will require a full thermodynamic and structural description of the binding of NusG within the ternary (NusG−Rho−RNAP) complex, but we note that the interaction of NusA with the *E. coli* transcription elongation complex in the presence and absence of the antitermination protein N of phage λ may represent a comparable system. Here also the functional consequences of NusA binding are quite different in the binary NusA−RNAP complex and the ternary NusA−N−RNAP complex (reviewed in *45*), since in the absence of N protein NusA serves to slow the average elongation rate of RNAP and enhance intrinsic termination, while in the presence of the N protein NusA serves to increase the rate of elongation and promote N-dependent antitermination.

It is tempting to build on the above results and earlier studies to speculate more explicitly on how NusG binding might perturb the function of the *E. coli* RNAP within the transcription complex. Erie et al. (*46*) presented evidence, based on experiments in which nucleotide misincorporation rates were measured, that the elongation of *E. coli* RNAP can be described by a branched kinetic scheme. In this model, the RNAP in the elongation complex can assume two or more states at each template position, depending on the relative rates of formation of alternative transcription complex conformations. More recent interpretations of these results (see *1*) suggest that these competing conformations may represent either a fully functional elongation complex in which the 3′-terminus of the nascent RNA remains bound to the active site of the RNAP, or a "slid-back" complex in which the 3′-terminus of the RNA has been released from the active site. Elongation factors GreA and GreB drive the transition from the slid-back complex to the elongation-competent complex by facilitating the cleaving of one or more nts from the extruded 3′-end of the nascent RNA. This cleavage reaction facilitates the rebinding of the (newly formed) 3′-end of the nascent RNA chain to the active site of the enzyme, and thereby accelerates the re-formation of elongation-competent complexes. Thus, it appears that the elongation complex has an inherent propensity to fluctuate between (at least) two conformational states, which can be designated "elongation-competent" and "slid-back" (and elongation-incompetent), respectively.

Komissarova and Kashlev (*47*) and Nudler et al. (*48*) showed that *E. coli* RNAP can slide upstream on the DNA template with no concomitant release or cleavage of either NTPs or the nascent RNA. This seems a common feature of RNA polymerases because human RNA polymerase II also has been shown to undergo arrest and backsliding into an inactive state (*49*). For RNAP II, the inactive state can be converted into an active (or elongation-competent) state by the action of elongation factor SII, which helps to bring about the cleavage of the nascent RNA chain and probably facilitates placement of the new 3′-end in the appropriate enzymic site for elongation. In the slid-back state, the 3′-end of the RNA is thought to be released from the active site of the enzyme, and sliding upstream on the DNA template does not involve a reversal of the polymerization reaction. Thus, the fact that *E. coli* and transcription complexes can slide on the DNA without RNA dissociation or hydrolysis also argues that the RNAP−DNA−nascent RNA ternary complex can exist in more than one state.

Because NusG induces Rho-dependent termination at upstream template positions and does not seem to affect the processivity and translocation rate of Rho, it is reasonable to argue that, in either the presence or the absence of NusG, Rho is poised to terminate at these positions. Stated differently, although Rho is thought to be present at the elongation complexes at the appropriate upstream termination locations, it cannot, in the absence of NusG, lower the energetic barrier to RNAP termination (or increase the barrier to elongation) and therefore cannot bring about termination at these upstream positions. This notion is supported by experiments performed by Zhu (*50*), who observed that a significantly reduced fraction of RNA could be released by Rho from stalled elongation complexes at many *trp t′* template positions, compared to the fraction of RNA released by Rho from actively transcribing complexes at the same template positions. Prolonged incubation of stalled elongation complexes resulted in a further decrease in the fraction of Rho-sensitive complexes, arguing that as more complexes became elongation-incompetent they also became Rho-insensitive. In contrast, the fraction of stalled complexes that remained elongation-competent (as defined by activity in the "chase" reactions) also remained Rho-sensitive.

Based on the above considerations, it is tempting to hypothesize that at NusG-sensitive template sites the elongation complex exists mostly in a Rho-resistant, elongation-incompetent (slid-back?) state, which can become elongation-competent in the presence of NusG. Because NusG increases the elongation rate of *E. coli* RNAP, it seems reasonable to suggest that NusG shifts the conformational equilibrium of the complexes toward the elongation-competent state. In the Rho-dependent termination reaction, NusG would exert its effect by facilitating transition of the elongation complex from the Rho-resistant, elongation-incompetent state to the Rho-sensitive, elongation-competent state. This mechanism is shown schematically in Figure 7.

Incorporation of NusA Effects into the Overall Model for Rho-Dependent Termination. The activity of another *nus* factor, NusA, also can be described in the context of the model presented in Figure 7. NusA forms a complex with elongating *E. coli* RNAP, with $K_d \sim 10^{-7}$ M (*51*). In contrast to NusG, which accelerates the average rate of RNA elongation by 25−30% (*16*, *17*), NusA slows the average rate of elongation by 20−35% (*17*, *52*). A related NusA activity is the enhancement of natural pause sites and formation of new ones (*8*, *53*, *54*). In addition to throttling down the rate of transcription by *E. coli* RNAP, NusA also decreases the efficiency of Rho-dependent termination at the phage λ *tR1* (*53*) and the *E. coli lacZ* genes (*17*). As discussed by Zhu and von Hippel (*11*) and Burns et al. (*17*), these activities cannot be explained by the original simple kinetic coupling model of Rho-dependent termination (*7*), but they can be explained by the model for the regulation of Rho-dependent termination by NusG, presented in Figure 7.

In contrast to NusG, NusA can be thought to work by shifting the conformational equilibrium of the elongation complex at each template position from the elongation-competent state toward the elongation-incompetent, slid-back state. Because elongation does not proceed in the slid-back

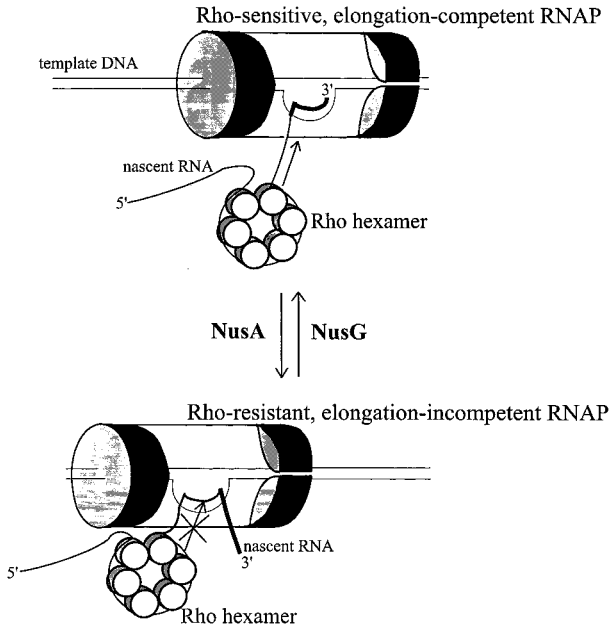

FIGURE 7: Model for the competing functions of NusG and NusA in Rho-dependent termination. *E. coli* elongation complexes can fluctuate between two or more functional (and conformational) states. We suggest that NusG may produce its effects on Rho-dependent termination by favoring the elongation-competent state, while NusA may operate by stabilizing the elongation-incompetent (slid-back) state (see text). A portion of the nascent RNA is represented by thicker lines to illustrate the sliding-back of the transcription complex relative to the RNA (and DNA) components of the complex.

state, this model can explain both the pausing enhancement and elongation-rate-decreasing activities of NusA. In addition, the inhibition of Rho-dependent termination by NusA can be explained if Rho acts on elongation-competent, but not on slid-back RNAP. Given our increased understanding of the different elongation states of *E. coli* RNAP, this model can now can be tested more directly.

Other Roles of NusG in Transcription Elongation. NusG is involved in transcription elongation activities that are not related to Rho-dependent termination. These activities also are likely to reflect direct interactions between NusG and the RNAP of the *E. coli* transcription complex. We summarize these activities here for completeness, since these interactions may be similar to those responsible for the regulation of Rho-dependent termination by NusG. First, NusG and Rho participate in the process of N protein-dependent antitermination that is involved in triggering the lytic state of phage λ in *E. coli.* In this system, both NusG and Rho form a part of the host-protein-containing antitermination subassembly that stabilizes the interaction of N protein with the RNAP of *E. coli* and projects the antitermination effect of N further downstream of the regulatory *nut* sequence along the template (*55*, and references cited within). Based on the results of our present study, it is possible that NusG participates in this antitermination assembly in the form of a 1:6 NusG-Rho complex.

In addition, NusG and the phage HK022 Nun protein are involved in transcription termination near the phage λ *nut* site (*56, 57*). This activity results in transcription of HK022 but not λ DNA, and eventually the exclusion of λ by HK022. Isolation of NusG mutants defective in Nun-dependent termination, but not in Rho-dependent termination, suggests that these activities are distinct and that Rho may not be required for Nun-dependent termination near the λ *nut* site (*57*). Finally, as pointed out above, NusG alone can increase the elongation rate of the transcription complex of *E. coli* (*16, 17*). Since the NusG−RNAP interaction may be weak in the absence of Rho, this elongation-enhancement activity of NusG could be significantly greater under conditions of NusG saturation. This notion is supported by the experiments of Burova and Gottesman (*58*), who showed that overexpression of NusG inhibits Rho-dependent termination at the phage λ *tR1* and *tL1* termination regions. When Rho also was overexpressed, however, wild-type termination at these sites was restored, arguing that maintenance of the appropriate ratio of these two proteins is essential for the correct regulation of transcription.

ACKNOWLEDGMENT

We thank C. Conant for insightful suggestions on experimental design and critical reading of the manuscript, and all other members of our laboratory for stimulating discussions and experimental help. We thank the RASMB (Reversible Association in Structural and Molecular Biology) community for helpful discussions on analytical ultracentrifugation, and especially W. Stafford (Boston Biomedical Research Institute) for maintaining the Internet site (http://www.bbri.org/rasmb/rasmb.html) and mailing list, to the benefit of all members of this group.

REFERENCES

1. von Hippel, P. H. (1998) *Science 281*, 660−665.
2. Roberts, J. W. (1969) *Nature 224*, 1168−1174.
3. Richardson, J. P. (1996) *J. Biol. Chem. 271*, 1251−1254.
4. Platt, T. (1994) *Mol. Microbiol. 11*, 983−990.
5. Platt, T., and Richardson, J. P. (1992) in *Transcriptional Regulation* (McKnight, S. L., and Yamamoto, K. R., Eds.) pp 365−389, Cold Spring Harbor Laboratory Press, Cold Spring Harbor, NY.
6. Bear, D. G., and Peabody, D. S. (1988) *Trends Biochem. Sci. 13*, 343−347.
7. Jin, D. J., Burgess, R. R., Richardson, J. P., and Gross, C. A. (1992) *Proc. Natl. Acad. Sci. U.S.A. 89*, 1453−1457.
8. Kassavetis, G., and Chamberlin, M. J. (1981) *J. Biol. Chem. 256*, 2777−2786.
9. Zhu, A. Q., and von Hippel, P. H. (1998) *Biochemistry 37*, 11202−11214.
10. Brennan, C. A., Dombroski, A. J., and Platt, T. (1987) *Cell 48*, 945−952.
11. Zhu, A. Q., and von Hippel, P. H. (1998) *Biochemistry 37*, 11215−11222.
12. Walstrom, K. M., Dozono, J. M., Robic, S., and von Hippel PH. (1997) *Biochemistry 36*, 7980−7992.
13. Walstrom, K. M., Dozono, J. M., and von Hippel PH. (1997) *Biochemistry 36*, 7993−8004.
14. Downing, W. L., Sullivan, S. L., Gottesman, M. E., and Dennis, P. P. (1990) *J. Bacteriol. 172*, 1621−1627.
15. , Li, J., Horwitz, R., McCracken, S., and Greenblatt, J. (1992) *J. Biol. Chem. 267*, 6012−6019.
16. Burova, E., Hung, S. C., Sagitov, V., Stitt, B. L., and Gottesman, M. E. (1995) *J. Bacteriol. 177*, 1388−1392.
17. Burns, C. M., Richardson, L. V., and Richardson, J. P. (1998) *J. Mol Biol. 278*, 307−316.
18. Sullivan, S. L., and Gottesman, M. E. (1992) *Cell 68*, 989−994.
19. Burns, C. M., and Richardson, J. P. (1995) *Proc. Natl. Acad. Sci. U.S.A. 92*, 4738−4742.
20. Nehrke, K. W., Zalatan, F., and Platt, T. (1993) *Gene Expression 3*, 119−133.

21. Nehrke, K. W., and Platt, T. (1994) *J. Mol. Biol. 243*, 830−839.
22. Walstrom, K. M., Dozono, J. M., and von Hippel, P. H. (1998) *J. Mol. Biol. 279*, 713−726.
23. Laemmli, U. K. (1970) *Nature 227*, 680−685.
24. Van Holde, K. E., and Weischet, W. O. (1978) *Biopolymers 17*, 1387−1403.
25. Stafford, W. F., III (1992) *Anal. Biochem. 203*, 295−301.
26. Burgess, R. S., and Jendrisak, J. J. (1975) *Biochemistry 14*, 4634−4638.
27. Li, J., Mason, S. W., and Greenblatt, J. (1993) *Genes Dev. 7*, 161−172.
28. Geiselmann, J., Yager, T. D., Gill, S. C., Calmettes, P., and von Hippel, P. H. (1992) *Biochemistry 31*, 111−121.
29. Geiselmann, J., Seifried, S. E., Yager, T. D., Liang, C., and von Hippel, P. H. (1992) *Biochemistry 31*, 121−132.
30. Nehrke, K. W., Seifried, S. E., and Platt, T. (1992) *Nucleic Acids Res. 20*, 6107.
31. Hansen, J. C., Lebowitz, J., and Demeler, B. (1994) *Biochemistry 33*, 13155−13163.
32. Jonsson, U., Fagerstam, L., Ivarsson, B., Johnsson, B., Karlsson, R., Lundh, K., Lofas, S., Persson, B., Roos, H., Ronnberg, I., Sjolander, S., Stenberg, E., Stahlberg, R., Urbaniczky, C., Ostlin, H., and Malmqvist, M. (1991) *BioTechniques 11*, 620−627.
33. Morton, T. A., and Myszka, D. G. (1998) *Methods Enzymol. 295*, 268−294.
34. Geiselmann, J., Yager, T. D., and von Hippel, P. H. (1992) *Protein Sci. 1*, 861−873
35. Myszka, D. G., He, X., Dembo, M., Morton, T. A., and Goldstein, B. (1998) *Biophys. J. 75*, 583−594.
36. Yoo, S., Myszka, D. G., Yeh, C., McMurray, M., Hill, C. P., and Sundquist, W. I. (1997) *J. Mol. Biol. 269*, 780−795.
37. Myszka, D. G., Morton, T. A., Doyle, M. L., and Chaiken, I. M. (1997) *Biophys. Chem. 64*, 127−137.
38. Joss, L., Morton, T. A., Doyle, M. L., and Myszka, D. G. (1998) *Anal. Biochem. 261*, 203−210.
39. Wu, A. M., Christie, G. E., and Platt, T. (1981) *Proc. Natl. Acad. Sci. U.S.A. 78*, 2913−2917.
40. Levin, J. R., Krummel, B., and Chamberlin, M. J. (1987) *J. Mol. Biol. 196*, 85−100.
41. Daube, S. S., and von Hippel, P. H. (1994) *Biochemistry 33*, 340−347.
42. Uptain, S. M., Kane, C. M., and Chamberlin, M. J. (1997) *Annu. Rev. Biochem. 66*, 117−172.
43. Burns, C. M., Nowatzke, W. L., and Richardson, J. P. (1999) *J. Biol. Chem. 274*, 5245−5251.
44. Washburn, R. S., Jin, D. J., and Stitt, B. L. (1996) *J. Mol. Biol. 260*, 347−358.
45. Das, A. (1993) *Annu. Rev. Biochem. 62*, 893−930.
46. Erie, D. A., Hajiseyedjavadi, O., Young, M. C., and von Hippel, P. H. (1993) *Science 262*, 867−873.
47. Komissarova, N., and Kashlev, M. (1997) *Proc. Natl. Acad. Sci. U.S.A. 94*, 1755−1760.
48. Nudler, E., Mustaev, A., Lukhtanov, E., and Goldfarb A. (1997) *Cell 89*, 33−41.
49. Reeder, T. C., and Hawley, D. K. (1996) *Cell 87*, 767−777.
50. Zhu, A. Q. (1997) Ph.D. Dissertation, pp 135−179, Department of Chemistry, University of Oregon.
51. Gill, S. C., Weitzel, S. E., and von Hippel, P. H. (1991) *J. Mol. Biol. 220*, 307−324.
52. Rees, W. A., Weitzel, S. E., Das, A., and von Hippel, P. H. (1997) *J. Mol. Biol. 273*, 797−813.
53. Lau, L. F., Roberts, J. W., and Wu, R. (1983) *J. Biol. Chem. 258*, 9391−9397.
54. Landick, R., and Yanofsky, C. (1984) *J. Biol. Chem. 259*, 11550−11555.
55. Mogridge, J., Mah, T. F., and Greenblatt, J. (1998) *J. Biol. Chem. 273*, 4143−4148.
56. Hung, S. C., and Gottesman, M. E. (1995) *J. Mol. Biol. 247*, 428−442.
57. Burova, E., Hung, S. C., Chen, J., Court, D. L., Zhou, J. G., Mogilinitskiy, G., and Gottesman, M. E. (1999) *Mol. Microbiol. 31*, 1783−1793.
58. Burova, E., and Gottesman, M. E. (1995) *Mol. Microbiol. 17*, 633−641.

BI992658Z